Soils and Rocks
An International Journal of Geotechnical and Geoenvironmental Engineering
www.soilsandrocks.com
ISSN 1980-9743
ISSN-e 2675-5475

Floating stone column-supported embankments on soft soils: numerical study incorporating stability analysis and basal reinforcement with geosynthetic

José Leitão Borges[1#]

Article

Keywords
Floating stone columns
Embankment
Soft soil
Geosynthetic
Overall stability
Mechanical-hydraulic coupled analysis

Abstract

Although fully penetrating stone columns have widely been studied in the literature, the number of published studies on floating stone columns – which also have been efficiently used to improve vertically lengthy soft-clay deposits – is very limited. Basal reinforcement with geosynthetic is another technique that increases overall stability of embankments on soft soils and can be combined with stone columns. In the paper, mechanical-hydraulic coupled finite element analyses are performed to study a floating stone column-supported embankment on a thick soft soil deposit. A parametric analysis is conducted so that the influence of two governing factors is evaluated: length of stone columns; basal reinforcement with geosynthetic. An overall stability analysis method, which uses the results of finite element analyses, is also applied. Results of several key variables are analysed: overall safety factor, settlements, horizontal displacements, vertical stress at the embankment base, stress concentration ratio, excess pore pressures and geosynthetic tensile force.

1. Introduction

Stone columns have widely been studied in the literature due to their advantages in efficiently improving soft soils during the construction of embankments of railway or road infrastructures. This technique is one of the most adequate when the main purpose is, simultaneously, to increase overall stability and reduce and accelerate settlements.

Although most experimental and numerical studies published in the literature concern fully penetrating stone columns (i.e., end-bearing stone columns, with their tip lying on the lower hard stratum) (e.g. Borges et al., 2009; Chen et al., 2009, 2013; Castro & Sagaseta, 2011; Elsawy, 2013; Almeida et al., 2015; Basack et al., 2017; Castro, 2017; Marques & Borges, 2018a,b; Miranda et al., 2021; Zhou et al., 2021; Zhang et al., 2022; Chen et al., 2022), floating stone columns have also efficiently been used in vertically lengthy soft-clay deposits (Chen et al., 2022) and can reduce cost. However, the number of published studies of floating stone columns is very small.

When floating stone columns are used to reinforce a very thick soft soil deposit, it should be considered that the length of columns determines opposite effects on the cost and structural improvement. Therefore, an adequate length of columns should be defined so that the cost-improvement binomial is as optimized as possible.

Basal reinforcement with geosynthetic is another technique that also increases overall stability of embankments on soft soils (Rowe & Soderman, 1985, 1987; Borges & Cardoso, 2002; Rowe & Li, 2005) and can be combined with stone columns to further increase short-term safety against overall failure.

Although many studies have been published on stone column-supported embankments, the number of studies where basal reinforcement of geosynthetic is combined with stone columns is much smaller. Deb et al. (2011) presented laboratory model tests on unreinforced and geogrid-reinforced stone column-improved soft clay; the results showed that the inclusion of the geogrid increased the load-carrying capacity and decreased the settlement of the soil. Using the concept of the cylindrical unit cell to model the behaviour of a geosynthetic-reinforced and column-supported embankment, Zhao et al. (2019) proposed a closed-form solution applied to columns close to the middle section of the embankment and showed that the inclusion of a geosynthetic reinforcement can increase the load transfer efficiency into the columns.

Zhang et al. (2022), using a finite element model, performed a parametric study of floating geosynthetic-encased stone column-supported embankments with geosynthetic basal reinforcement. The effects of the consistency of substratum soil (soil underlying the column tip), tensile stiffness of basal reinforcement and encasement were analysed. The results

#Corresponding author. E-mail address: leitao@fe.up.pt
[1]Universidade do Porto, Construct, Faculdade de Engenharia, Porto, Portugal.

Submitted on May 16, 2023; Final Acceptance on July 9, 2024; Discussion open until February 28, 2025.
https://doi.org/10.28927/SR.2024.006023

showed that higher embankment loads were transferred to the surrounding soft soil when the stone columns were constructed on a weaker substratum. Larger settlements at embankment crest, ground surface and the plane of column bottom were also obtained, as well as higher tensile strains of the basal reinforcement and lateral displacements of columns. The increase of encasement stiffness resulted in a decrease in the global settlement and restricted the increase of lateral displacements and tensile strains in the basal reinforcement. When the stiffness of basal reinforcement increased, larger embankment load was transferred to the floating columns and lower lateral displacements was obtained.

Centrifuge tests and numerical modelling were also conducted by Chen et al. (2022) regarding a geosynthetic-reinforced and floating encased stone column-supported embankment. The results illustrated that the inclusion of the basal reinforcement significantly reduced total and uneven settlement at the embankment crest and base, as well as lateral displacement at the top of the column; however, the lateral displacement at the bottom of the floating columns increased.

In this paper, a fully mechanical-hydraulic coupled finite element code is applied to perform a parametric study on the behaviour of a floating stone column-supported embankment on a thick soft soil deposit. Two parameters are studied: length of columns (the effect of its variation is analysed in cases without basal reinforcement); basal reinforcement with geosynthetic (for a particular length of floating columns, different constitutive curves are considered for the geosynthetic). Results of several main variables are analysed, namely: overall safety factor, settlements, horizontal displacements, vertical stress at the embankment base, stress concentration ratio, excess pore pressures and geosynthetic tensile force. The overall safety factor is computed applying a stability analysis method (computer code) which uses the numerical results of the finite element code, as explained below.

2. Computer codes

2.1 Finite element model

The finite element code, developed by Borges (1995), incorporates, among other aspects, the following features applied in this study: (i) fully mechanical-hydraulic coupled analysis; (ii) the *p-q-θ* critical state model for soil constitutive behaviour simulation (Borges, 1995; Lewis & Schrefler, 1987); (iii) hardening elastoplastic models to simulate constitutive behaviours of the geosynthetic and soil-geosynthetic interfaces (Borges, 1995; Borges & Cardoso, 2001). Subsequently to the initial version of the code (two-dimensional modelling version), several other improvements were also developed and implemented, particularly a three-dimensional modelling version (Borges, 2004).

For two-dimensional (2D) analysis, two types of the six-noded triangular element (nodes at the vertices and middle of the sides) are used: (i) coupled element, for the soft soil, where consolidation is considered (all the six nodes have displacement degrees of freedom while only the three vertex nodes have excess pore pressure degrees of freedom). (ii) non-coupled element, for stone columns and embankment material (all the six nodes have only displacement degrees of freedom). Bar and interface elements are used to model the geosynthetic and soil-geosynthetic interfaces, respectively.

The *p-q-θ* model is an extension of the Modified Cam-Clay model into the three-dimensional stress space which uses the Mohr-Coulomb surface as the critical state criterion. This means that the parameter that defines the slope of the critical state line, M, is not constant (as happens in the Modified Cam-Clay model) and depends on the angular stress invariant θ and effective friction angle, ϕ', as follows:

$$M = \frac{3\sin\varphi'}{\sqrt{3}\cos\theta + \sin\varphi'\sin\theta} \quad (1)$$

Therefore, the critical state line (Mohr-Coulomb criterion) is defined when M, given by Equation 1, is introduced in the following equation:

$$q = M.p \quad (2)$$

where q is the deviatoric stress and p is the effective mean stress.

The finite element code has been applied to analyse a large range of geotechnical structures involving fully mechanical-hydraulic coupled modelling (e.g., Borges, 1995, 2022; Domingues, 2006; Costa et al., 2007; Marques, 2008; Borges & Cardoso, 2001, 2002; Borges & Almeida, 2018; Borges & Guerra, 2014; Borges et al., 2009; Borges & Marques, 2011; Borges & Gonçalves, 2016; Borges & Santos, 2020; Marques, 2021). Several case studies were modelled and, comparing field and numerical results, good agreements were obtained, namely in: (i) two embankments on soft soils reinforced with stone columns, one in the Gold Coast Highway of Australia (Marques, 2021), and the other in the northern railway of Portugal (Domingues, 2006) (ii) two trial geosynthetic-reinforced embankments on soft soils (Borges, 1995), one constructed up to failure and the other observed until the end of consolidation; (iii) a braced excavation in very soft ground carried out in the City of San Francisco (Costa et al., 2007; Costa, 2005).

2.2 Stability analysis code

The overall stability analysis code applied in this study was developed by Borges (1995) and uses the results of the finite element model mentioned above. It was also presented and applied in Borges & Cardoso (2002) and was specifically developed for embankments on soft soils

with basal reinforcement with geosynthetics. It can also be efficiently applied when stone columns are used or basal reinforcement is not included.

For any phase of the problem, the stability analysis code computes the overall safety factor, F, with the results of the finite element code (2D coupled analysis). A large number of potential slip circular cylindrical surfaces is analysed so that the critical slip circle is obtained, which corresponds to the smallest value of F calculated.

For a particular potential slip circle, the intersection points of the circle with the sides of the 2D finite elements (six-noded triangular elements) are determined. Thus, the slip circle is divided into small straight-line segments, each of them located inside of only one of the 2D finite elements of the mesh. Intersection of the slip circle with the geosynthetic (or geosynthetics, if there are several reinforcement layers) modelled by bar elements is also determined (Figure 1).

Therefore, for the slip circle divided into small segments, the overall safety factor is calculated with the following equation (Borges, 1995; Borges & Cardoso, 2002):

$$F = \frac{\sum_{i=1}^{N} q_{fi} l_i + \sum_{j=1}^{N_g} \left[T_{rj} \cos(c_r \theta_j) \right]}{\sum_{i=1}^{N} \tau_i l_i + \sum_{j=1}^{N_g} \left[T_{aj} \cos(c_r \theta_j) \right]} \quad (3)$$

where: N – number of 2D elements of the mesh intersected by the circle; l_i – i-segment length; q_{fi} – average value of soil shear strength at i-segment (calculated using formulations of the critical state soil mechanics, as indicated below); τ_i – average value of acting shear stress at i-segment (determined from effective stresses σ'_x, σ'_y and τ_{xy}, known the angle that defines i-segment inclination; xy – plane of the finite element analysis); N_g – number of geosynthetic layers (usually, N_g =1); T_{rj} – resisting tensile force of j-geosynthetic at cut point (intersection of the slip circle with the geosynthetic, point I in Figure 1); T_{aj} – acting tensile force of j-geosynthetic at the cut point I (obtained interpolating between the tensile stresses at the two nearest Gauss points of the bar element that contains point I); θ_j – angle between the geosynthetic and the tangent to the slip circle at the cut point; c_r – reduction coefficient (it ranges between 0 and 1; usually c_r=1, the most conservative assumption, which assumes that the geosynthetic remains in its original orientation).

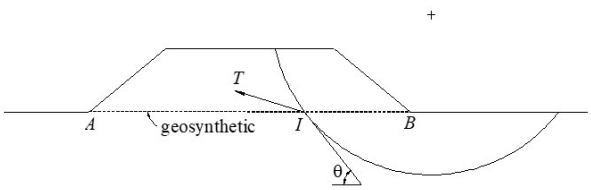

Figure 1. Intersection of the slip circle with the geosynthetic.

The calculation of resisting tensile force of geosynthetic at cut point, T_r, explained in detail in Borges & Cardoso (2002), is function not only of the geosynthetic strength (T_{rg}) but also of the maximum force that can be mobilised at point I considering the pull-out strength of the soil-geosynthetic interfaces (T_{rp}). T_r is the smaller value of these two strengths, i.e.:

$$T_r = \min(T_{rg}, T_{rp}) \quad (4)$$

Since the p-q-θ model is used in the finite element analysis, shear strength of soils is calculated by the following equation of the critical state soil mechanics (Britto & Gunn, 1987; Borges, 1995):

$$q_{fi} = \frac{1}{2} M . \exp\left(\frac{\Gamma - v_i}{\lambda} \right) \quad (5)$$

where M is obtained by Equation 1 and v_i, the specific volume of soil at i-segment, is computed as follows:

$$v_i = \Gamma - k \ln p_i - (\lambda - k) \ln \alpha_{pi} \quad (6)$$

At the i-segment, $p_i = (\sigma'_{xi} + \sigma'_{yi} + \sigma'_{zi})/3$ is the effective mean stress and α_{pi} is the p-value of the centre of the yield surface in p-q plane (Borges, 1995; Lewis & Schrefler, 1987), extrapolated from α_p-values at Gauss points of finite element; λ, k and Γ, parameters of the p-q-θ model (soil properties), are defined as follows: λ, slope of normal consolidation line and critical state line; k, slope of swelling and recompression line; Γ, specific volume of soil on the critical state line at mean normal stress equal to 1 kPa.

3. Numerical modelling

The problem concerns a 2.5-m-high symmetric embankment, with large longitudinal length, built on a 25-m-thick soft clay lying on a rigid and impermeable stratum (Figure 2). The width of the embankment crest is 12 m. Floating stone columns are installed in the soft soil, as shown in Figure 2. The water level is at the ground surface.

Due to the requirement of large computational time and complexity of the three-dimensional (3D) arrangement of multiple columns, the 3D problem of stone column-supported embankments has been commonly converted into a 2D model considering plane strain analysis. Two basic types of equivalency methods have been used: the equivalent

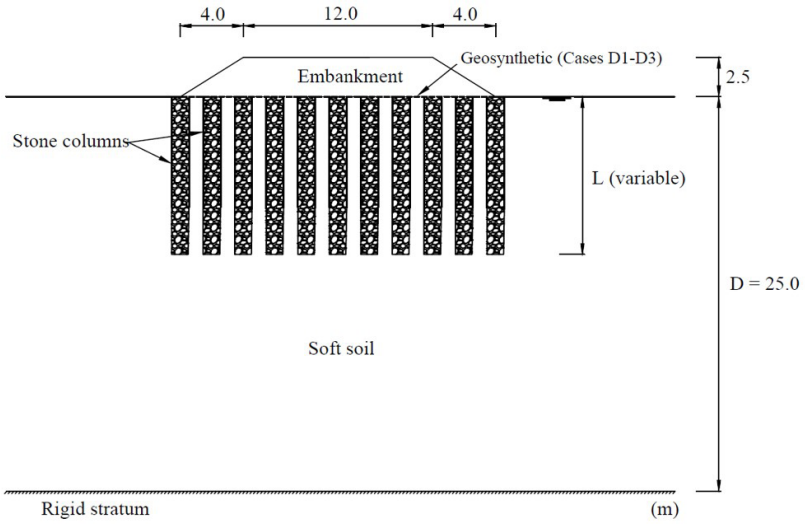

Figure 2. Cross-sectional view of the problem.

area method and the column-wall method (Marques, 2021; Castro, 2017; Marandi et al., 2016; Zhang et al., 2014; Abusharar & Han, 2011; Tan et al., 2008; Cooper & Rose, 1999; Christoulas et al., 1997).

In the equivalent area method, the stone columns and the surrounding soil are considered as a composite ground (also called an improved area), while, in the column-wall method, the columns are transformed into longitudinal stone walls (Figure 3). A column-wall model is adopted in this study with the following geometric parameters for the walls: wall thickness, 0.475 m; midplane-to-midplane spacing between walls, 2.0 m. This corresponds to individual columns with diameter of 1.1 m in a 3D arrangement with the same spacing (i.e. axis-to-axis spacing of 2.0 m) and equal value of the area replacement factor (a_s). The area replacement factor is defined as follows:

$$a_s = \frac{A_c}{A_t} \tag{7}$$

where A_c is the column area and A_t is the tributary area of natural soil for each column ($A_t = s^2$ for stone columns distributed in a square grid; s – axis-to-axis spacing between columns).

Figure 4 depicts the finite element mesh of the problem. Drained analysis is considered in the embankment material and stone walls while fully mechanical-hydraulic coupled analysis is modelled in the clay. The construction of the embankment is modelled by adding layers of elements at a uniform rate and is completed in an overall time of 7 days. The effective thickness of column-walls is taken as constant in time; i.e. possible partial filling of gravel voids with particles of soft soil as a result of water percolation during consolidation is not considered in the calculations.

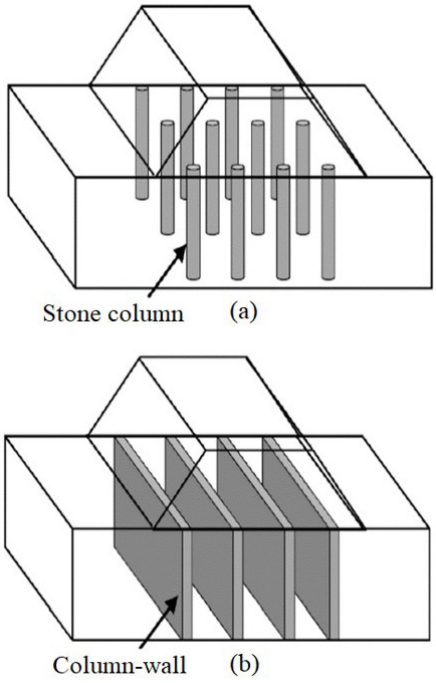

Figure 3. Embankment on soft soil supported by stone columns: (a) individual columns; (b) column-walls.

The following displacement boundary conditions are set: (i) zero-displacement in both x- and y-direction at y = 0 line, considering that the soft clay lays on a rigid stratum; (ii) zero-displacement in x-direction at the nodes of the symmetry axis ($x = 0$); (iii) zero-displacement in x-direction at the x = 41 m line (lateral boundary), assuming that the horizontal displacement can be set as zero at nodes which are enough distant from the embankment.

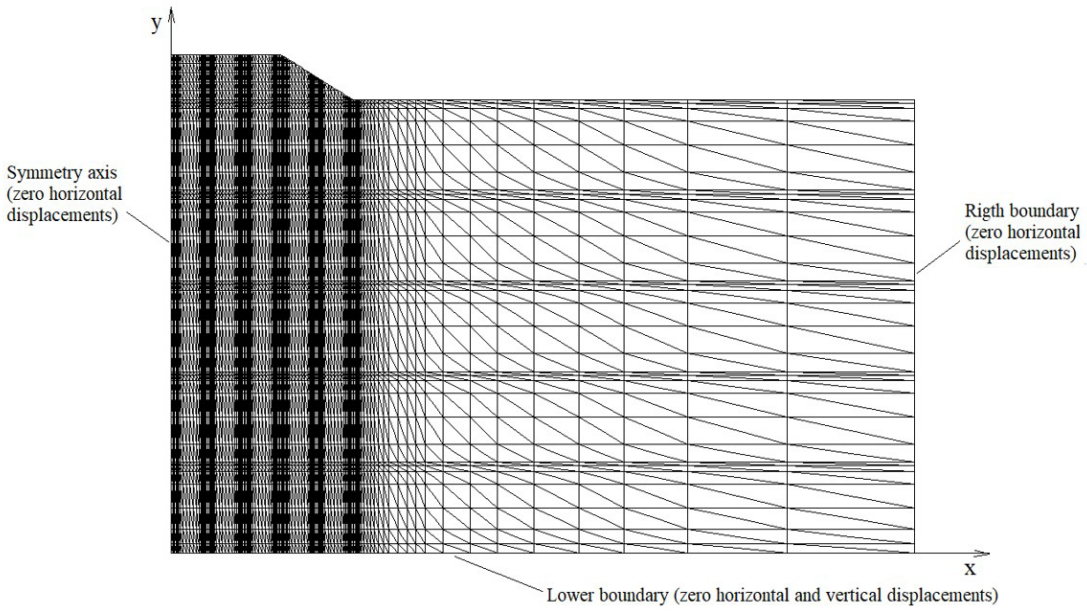

Figure 4. Finite element mesh.

Table 1. Geotechnical properties of the clay, embankment soil and stone column.

	γ (kN/m^3)	ν'	ϕ' (º)	k_h (m/s)	k_v (m/s)	*p-q-θ* critical state model			
						λ	k	Γ	N
Clay	16	0.25	26	10^{-9}	10^{-9}	0.18	0.025	3.05	3.158
Embankment	20	0.30	35	-	-	0.03	0.005	1.80	1.817
Stone column	17	0.30	40	-	-	0.0038	0.00095	1.914	1.916

Regarding the drainage boundary conditions, excess pore pressure is set as zero on the ground surface (y = 25 m plane) and on the lateral surfaces and tip of the column-walls.

The constitutive behaviour of the soils (clay, stone columns and embankment material) is simulated by the *p-q-θ* critical state model whose parameters are shown in Table 1 (λ, slope of normal consolidation line and critical state line; k, slope of swelling and recompression line; N, specific volume of normally consolidated soil at mean normal effective stress equal to 1 kPa; Γ, specific volume of soil on the critical state line at mean normal effective stress equal to 1 kPa). Other geotechnical properties are also indicated in Table 1: γ, unit weight; ϕ', angle of friction defined in effective terms; ν', Poisson's ratio for drained loading; k_h and k_v, coefficients of permeability in horizontal and vertical directions. The parameters of stone columns are based on those of stone columns constructed in soft ground of a railway infrastructure in Portugal (Domingues, 2006). The parameters of the clay are similar to those considered by Finno et al. (1991) in a soft ground in Chicago, USA. The values adopted for the embankment material are the same as those used by Borges & Cardoso (2001) in an embankment on soft ground.

4. Parametric study

4.1 Influence of column length

In order to study the influence of this parameter, five lengths of stone columns are considered for the problem described in section 3, as indicated in Table 2. In cases C1-C4, floating stone columns are considered, i.e. their lengths are smaller than the vertical thickness of soft ground (25 m), while, in case C5, the length of columns is equal to the thickness of soft ground (fully penetrating stone columns). Basal reinforcement with geosynthetic is not considered in all cases C1-C5.

Figure 5 shows the effect of this parameter on settlements of embankment base, at the end of construction and end of consolidation. Figure 6 also depicts maximum settlement on the embankment base, at the end of consolidation, *versus* *L/D*, ratio of the column length to the vertical thickness of soft soil. As expected, these results show that the longer the stone columns, the smaller the settlements. However, the curve of figure 6 illustrates that, when *L/D* increases from

0.2 to 0.4, the maximum settlement reduces 13 cm (from 46 cm to 33 cm), while for higher values of *L/D* the rate of settlement reduction is significantly smaller; maximum settlement reduces 5 cm when *L/D* increases from 0.4 to 0.6, and only 1 cm when *L/D* increases from 0.6 to 0.8 and from 0.8 to 1.0. This means that, in terms of settlement improvement – and also considering the cost – the option for floating stone columns, with a length between 10 m and 15 m, would be adequate in practice for this problem.

Numbering the stone columns from the symmetry axis to the embankment toe, their axis *x*-coordinate are: column 1, $x = 0$; column 2, $x = 2$ m; column 3, $x = 4$ m; column 4, $x = 6$ m; column 5, $x = 8$ m; column 6, $x = 10$ m. The following results are depicted in Figures 7 and 8 for cases C1-C5: horizontal displacements under the embankment toe (x=10 m), at the end of construction (7th day) and end of consolidation (Figure 7); settlement *versus* time at midpoint between columns 1 and 2 on the embankment base (coordinates: $x = 1$ m; $y = 25$ m) (Figure 8). These results illustrate that: (i) like for settlements, the longer the stone columns, the smaller the horizontal displacements; (ii) however, the reduction of horizontal displacements is also significantly higher when

Table 2. Length of columns for the five analysed cases.

Case	Length of columns (m)	*L/D* (m)
C1	5	0.2
C2	10	0.4
C3	15	0.6
C4	20	0.8
C5	25	1.0

L – length of columns; *D* – vertical thickness of soft soil.

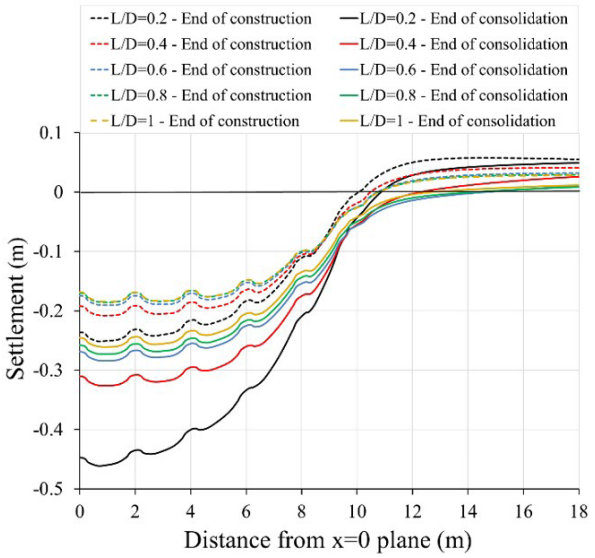

Figure 5. Influence of length of columns on vertical displacements of ground surface (embankment base), at the end of construction (7th day) and end of consolidation (cases C1-C5).

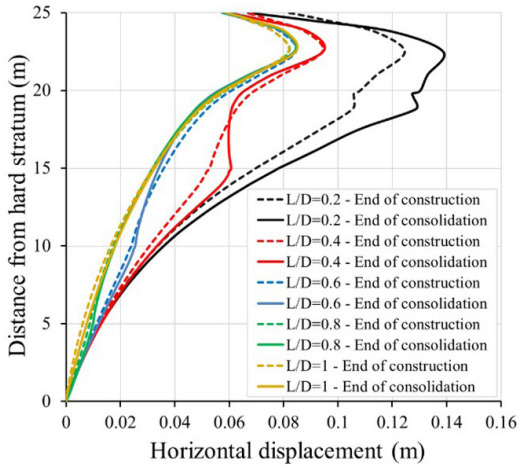

Figure 7. Influence of length of columns on horizontal displacements under the embankment toe (x =10 m), at the end of construction (7th day) and end of consolidation (cases C1-C5).

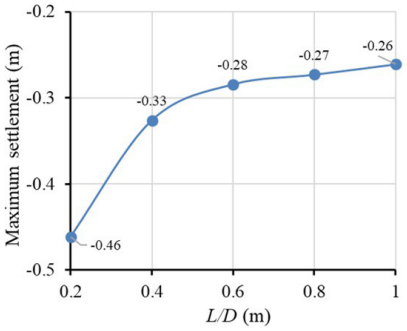

Figure 6. Influence of length of columns on maximum settlement at the embankment base (end of consolidation).

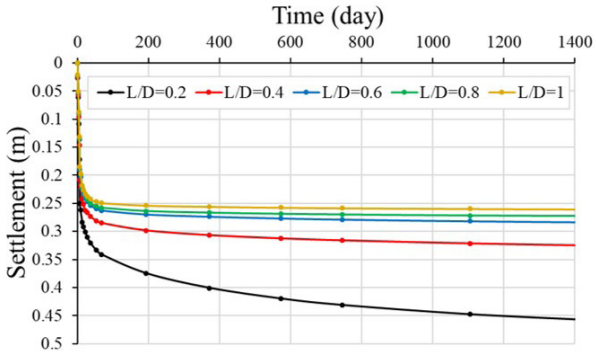

Figure 8. Settlement versus time at midpoint between columns 1 and 2 on the embankment base (coordinates: $x = 1$ m; $y = 25$ m) for cases C1-C5.

L/D increases from 0.2 to 0.4 than when *L/D* increases from 0.4 to larger values; (iii) due to the draining effect of stone columns, the longer the stone columns, the faster the rate of consolidation, as shown in Figure 8; however, again, the difference of consolidation rate between case C1 (*L/D*=0.2) and case C2 (*L/D*=0.4) is significantly larger than between case C2 and the other cases with longer stone columns.

In stone column-supported embankments on soft ground, since the columns have higher stiffness than the surrounding soft soil, the stone columns carry higher vertical stresses than the surrounding soil (or side soil, if column-walls are modelled, as in this study). This effect (arching effect) is shown in Figure 9 where vertical stress at the embankment base, for cases C1-C5, are depicted, at the end of construction and end of consolidation. Figure 10 also shows the stress concentration ratio on the top of the six columns. The stress concentration ratio, *SCR*, is a parameter that can also be used to evaluate the degree of stress concentration and is defined as the ratio of the average vertical stress on the column to that on its surrounding soil (or its corresponding side soil, if column-wall modelling is considered).

The results of these figures illustrate that, at the end of construction: (i) the stress concentration ratio (Figure 10a) assumes similar values in all five cases (C1-C5), except for column 6 (column under the embankment toe, which practically does not have embankment fill on its top); therefore, this means that the length of columns does not significantly influence the load transfer to the top of columns during construction; this fact is, somehow, understandable, since arching effect inside the embankment fill is essentially dependent on the vertical stiffness of foundation materials (stone columns and soft soil) and is directly related to respective differential settlements (between each column and its tributary soft soil) on the embankment base (which, at the end of construction, are similar, as shown in Figure 5); (ii) stress concentration ratio takes similar values in the four central columns (columns 1-4), while, in columns 5 and 6 (columns under the embankment slope), assumes higher values; this means that, although vertical stresses on top of columns 5 and 6 are lower than those on top of columns 1-4 (Figure 9), the magnitude of arching effect (ratio between stresses, on column and on tributary soft soil) is higher in the columns under the embankment slope; this effect is directly related to the lower horizontal confinement of columns 5-6 and their tributary soft soil, due to their position near the embankment toe – where horizontal displacements, shear stresses and stress levels are higher – determining a decrease of stiffness in the soft soil and stone columns, which affects the ratio between their stiffnesses and explains the above-mentioned differences in relation to the other columns. In response to consolidation, stress concentration ratio decreases a little in the central columns (columns 1-4) for all cases.

Figure 11 shows the influence of length of columns on the distributions of excess pore pressure at the end of

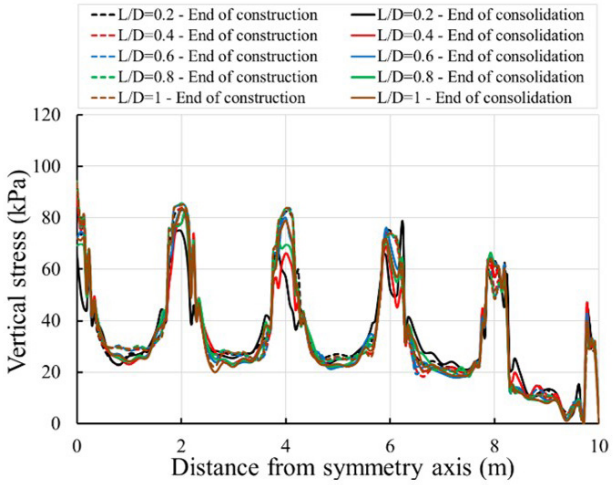

Figure 9. Influence of length of columns on vertical stress at the embankment base for cases C1-C5, at the end of construction (7th day) and end of consolidation.

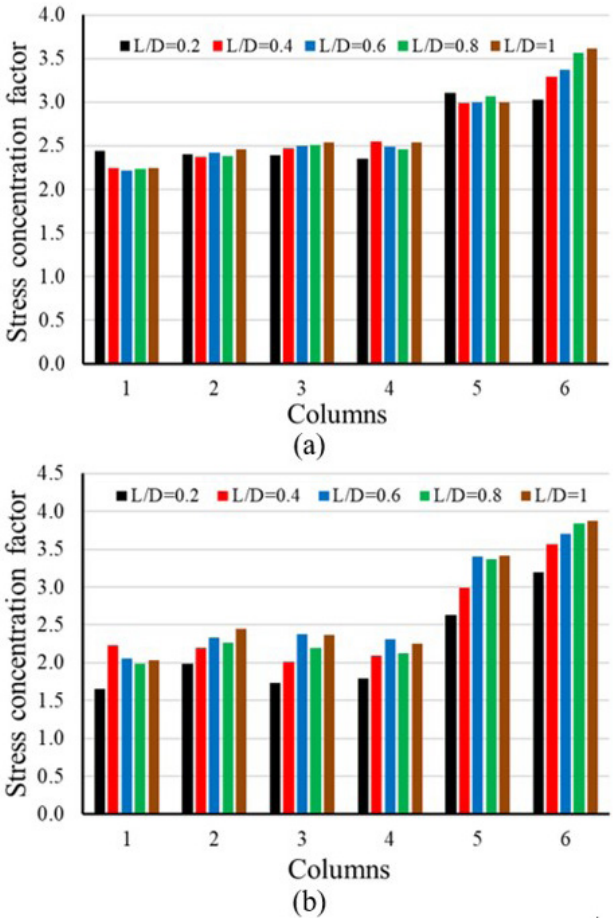

Figure 10. Influence of length of columns on the stress concentration ratio on the top of columns (cases C1-C5): a) end of construction; b) end of consolidation.

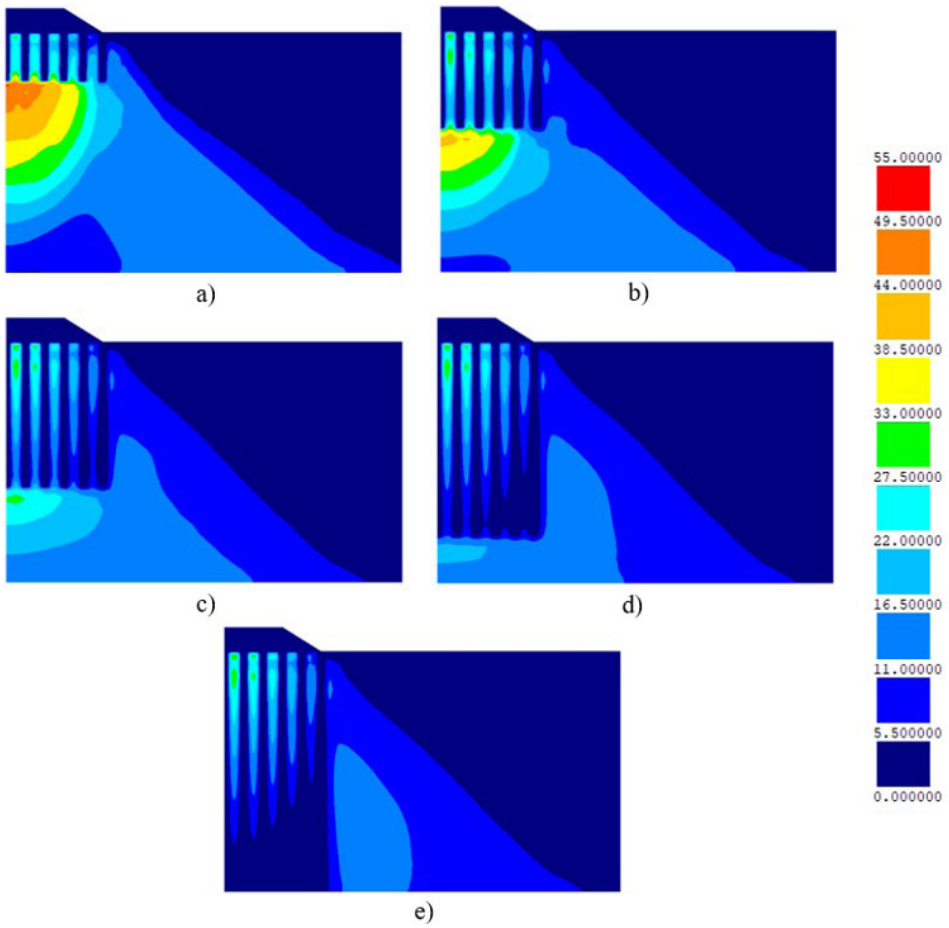

Figure 11. Influence of length of columns on excess pore pressure (u) at end of construction (7th day): a) L/D = 0.2 (u_{max} = 50.453 kPa); b) L/D = 0.4 (u_{max} = 40.234 kPa); c) L/D = 0.6 (u_{max} = 30.883 kPa); d) L/D = 0.8 (u_{max} = 30.991 kPa); e) L/D = 1.0 (u_{max} = 30.941 kPa).

construction (cases C1-C5). These results illustrate that, as expected, the shorter the columns, the higher the excess pore pressure at the end of construction, mainly below the end of columns; i.e. the shorter the columns, the higher the load transferred from the column to the soft soil on the column tip. However, like for displacements analysed above, while maximum value of excess pore pressure reduces from 50.5 kPa to 40.2 kPa when L/D increases from 0.2 to 0.4, for values of L/D higher than 0.6 the maximum value of excess pore pressure practically does not change.

The magnitude of excess pore pressures at the end of construction and vertical thickness of soft soil below the column tip are logically related with the magnitude of long-term settlements; i.e., due to consolidation after the end of construction, the higher the former, the larger the latter, as shown in Figures 5 and 11.

To analyse the effect of the length of columns on the overall stability of problem, Figure 12 depicts the critical slip surfaces – and respective overall safety factors – at the end of construction and end of consolidation, calculated from the finite element results with the computer code for stability analysis described in Section 2.2. Tables 3 and 4 also illustrate the sums of acting and resisting forces at the foundation (soft soil and stone columns) and at the embankment soil, along such critical surfaces, considering the application of Equation 3. It should be mentioned that, in addition to cases C1-C5, the same problem but without stone columns (i.e. L/D=0) was also modelled, which showed that, for such case, overall failure would occur (numerical instability and values of F lower than 1 were obtained before the completion of the embankment). This illustrated that some reinforcement or improvement technique would be needed in this problem, as considered in this studied.

Figure 12a and Table 3 show that the influence of the length of columns on the increase of overall stability at the end of construction is only effective for values of L/D lower than 0.4; i.e. F increases from 1.307 to 1.354 when L/D varies from 0.2 to 0.4, while, for values of L/D higher than 0.4, F remains without significant change (the critical slip surface is the same for cases C2-C5). This means that, like for settlements (as said above), in terms of overall stability improvement – and considering the cost – the option for

Table 3. Critical slip surfaces at the end of construction for cases C1-C5: overall safety factor (F) and sums of acting and resisting forces.

Case	X_0 (m)	Y_0 (m)	R (m)	Sum of acting forces (kN/m)		Sum of resisting forces (kN/m)		F
				Foundation $\sum_{i=1}^{N_1}\tau_i l_i$	Embankment $\sum_{i=1}^{N_2}\tau_i l_i$	Foundation $\sum_{i=1}^{N_1}q_{fi} l_i$	Embankment $\sum_{i=1}^{N_2}q_{fi} l_i$	(Eq. 3)
C1	8.5	31.5	12.671	239.49	5.470	305.18	15.027	1.307
C2	9.0	30.0	8.849	154.09	7.645	203.57	15.363	1.354
C3	9.0	30.0	8.849	153.35	7.526	203.28	16.259	1.365
C4	9.0	30.0	8.849	153.69	6.830	203.50	15.026	1.361
C5	9.0	30.0	8.849	153.71	7.171	203.35	15.465	1.360

R – radius; (X_0,Y_0) – coordinates of centre; $N=N_1+N_2$.

Table 4. Critical slip surfaces at the end of consolidation for cases C1-C5: overall safety factor (F) and sums of acting and resisting forces.

Case	X_0 (m)	Y_0 (m)	R (m)	Sum of acting forces (kN/m)		Sum of resisting forces (kN/m)		F
				Foundation $\sum_{i=1}^{N_1}\tau_i l_i$	Embankment $\sum_{i=1}^{N_2}\tau_i l_i$	Foundation $\sum_{i=1}^{N_1}q_{fi} l_i$	Embankment $\sum_{i=1}^{N_2}q_{fi} l_i$	(Eq. 3)
C1	9.5	31.5	11.769	210.63	-3.944	315.28	22.515	1.634
C2	9.5	28.0	6.536	124.45	2.680	181.68	15.506	1.551
C3	8.5	28.5	7.558	149.09	6.146	229.39	14.638	1.572
C4	10.0	28.5	7.123	121.81	5.465	183.97	16.673	1.576
C5	10.0	28.5	7.123	123.30	5.641	185.36	15.880	1.561

R – radius; (X_0,Y_0) – coordinates of centre; $N=N_1+N_2$.

floating stone columns, with a length between 10 m and 15 m, would also be adequate in practice for this problem.

At the end of consolidation, F takes a little higher value in case C1 (F=1.634) than in the other cases with longer stone columns, where F ranges between 1.551 and 1.576 (cases C2-C5). This is explained by the higher effect of consolidation on the increase of soft soil strength (larger reduction of soil volume provoking higher settlements) in case C1 determined by the larger values of excess pore pressure at the end of consolidation below the columns' tips, as shown above.

4.2 Influence of basal reinforcement with geosynthetic

In order to study the influence of this parameter, four cases with 10-m-long floating stone columns are considered: (i) case D0, which is equal to case C2, analysed in the previous section; therefore, basal reinforcement with geosynthetic is not included in this case; (ii) cases D1-D3, which are similar to case D0, but with geosynthetic reinforcement at the embankment base, where different constitutive curves are considered for the geosynthetic. All other parameters of the problem are kept equal in the four cases D0-D3.

Figure 13 illustrates the constitutive curves of the geosynthetic for cases D1-D3, which are simulated by an elastoplastic model, as explained below. These curves are similar to constitutive curves of three typical commercial geogrids. Considering different geosynthetics, it should be mentioned that their strength and stiffness are usually related to each other, i.e. the higher the geosynthetic stiffness, the higher its strength. This relation is therefore considered in this study. Respectively for cases D1, D2 and D3, the geosynthetic elastic modulus is 500 kN/m, 1000 kN/m and 1500 kN/m, and the geosynthetic strength, 50 kN/m, 100 kN/m and 150 kN/m; the geosynthetic thickness is considered equal to 2 mm in the three cases.

Soil-geosynthetic interfaces are modelled by interface elements. Their constitutive curve varies with the normal stress on the interface and is considered the same in the three cases, D1-D3. Figure 14 depicts the adopted curve for a normal stress of 15 kPa on the interface. The tangential stiffness of soil-geosynthetic interfaces takes the value of 1.6×10^4 kPa/m. Adhesion, a, and frictional angle, δ, for both upper and lower soil-geosynthetic interfaces are set as 0 kPa and 33.7º, respectively.

The elastoplastic models used to simulate the mechanical behaviours of the geosynthetic and soil-geosynthetic interfaces incorporate the following hardening law (Prevost & Hoeg, 1975; Owen & Hinton, 1980; Thomas, 1984; Borges, 1995):

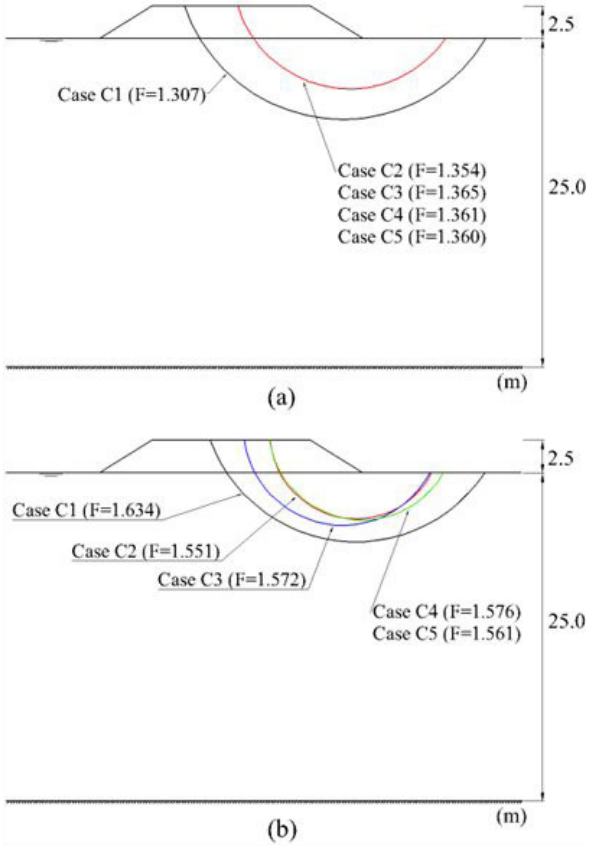

Figure 12. Critical slip surfaces for cases C1-C5: a) end of construction (7th day); b) end of consolidation.

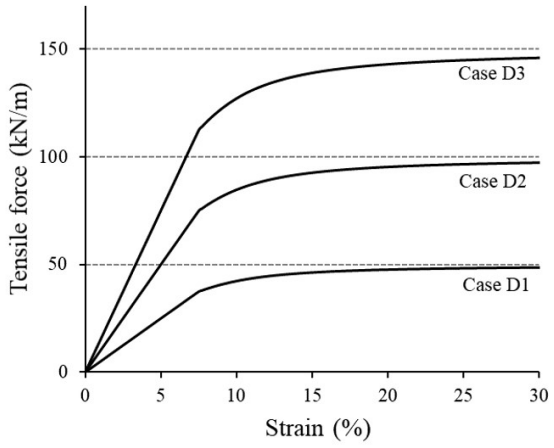

Figure 13. Constitutive curve of the geosynthetic for cases D1-D3.

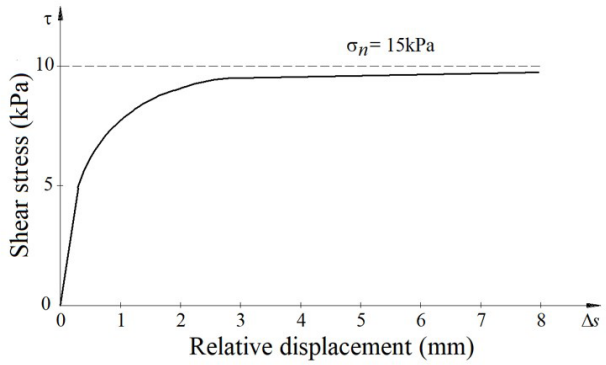

Figure 14. Constitutive curve of the soil-geosynthetic interfaces for normal stress of 15 kPa.

$$Y(h) = c_1 + \frac{c_2 h + c_3 h^2}{1 + c_4 h + c_5 h^2} \quad (8)$$

where h is the hardening parameter and c_1, c_2, c_3, c_4 and c_5 are constants that characterize a particular hardening curve. The following yielding function is used for the geosynthetic (Borges, 1995):

$$f = \sigma - Y(h) \quad (9)$$

where: σ – tensile stress; $Y(h) = \sigma_Y(\varepsilon_p)$ – hardening law; $h = \varepsilon_p$ – hardening parameter; σ_Y – yielding stress; ε_p – plastic tensile strain.

For the soil-geosynthetic interfaces, the yielding function is defined as follows (Borges, 1995):

$$f = |\tau| - \sigma_n Y(h) \quad (10)$$

where: τ – tangential stress; σ_n – normal stress; $Y(h) = \tan\delta(s_p)$ – hardening law; $h = \sum |s_p|$ – hardening parameter; δ – interface friction angle; s_p – plastic tangential relative displacement. More detailed descriptions of the implementation of these models are presented in Borges (1995). Values of c_1, c_2, c_3, c_4 and c_5 adopted for the geosynthetic and soil-geosynthetic interfaces are illustrated in Table 5, corresponding to the constitutive curves depicted in Figure 13 and 14, as said.

For cases D0-D3, Figure 15 shows the critical slip surfaces – and respective overall safety factors – at the end of construction and end of consolidation, calculated from the finite element results with the computer code for stability analysis described in Section 2.2. Taking into account the application of Equation 3, Tables 6 and 7 depict the sums of acting and resisting forces at the foundation (soft soil and stone columns) and at the embankment soil, along such critical surfaces, as well as the geosynthetic acting force T_a, the geosynthetic strength T_{rg}, the pull-out strength of the soil-geosynthetic interfaces T_{rp} and angle θ at its cut point. The reduction coefficient c_r is taken equal to 1, the most conservative option, as said above.

These results reveal that the safety factor (F) at the end of construction significantly increases when basal reinforcement with geosynthetic is included (cases D1-D3). As expected, the higher the geosynthetic strength, the higher the safety

Table 5. Hardening law constants.

	Case	c_1	c_2	c_3	c_4	c_5
geosynthetic	D1	18750 (kPa)	265625 (kPa)	0 (kPa)	42.5	0
	D2	37500 (kPa)	531250 (kPa)	0 (kPa)	42.5	0
	D3	56250 (kPa)	796875 (kPa)	0 (kPa)	42.5	0
soil-geosynthetic interface	D1-D3	0.333	417.094 (m^{-1})	0 (m^{-2})	1251.408 (m^{-1})	0 (m^{-2})

Table 6. Critical slip surfaces at the end of construction for cases D0-D3: overall safety factor (F) and sums of acting and resisting forces.

Case	X_0 (m)	Y_0 (m)	R (m)	Sum of acting forces (kN/m)			Geosyn. θ (°)	Sum of resisting forces (kN/m)				F
				Found. $\sum_{i=1}^{N_1}\tau_i l_i$	Embank. $\sum_{i=1}^{N_2}\tau_i l_i$	Geosyn. T_a		Found. $\sum_{i=1}^{N_1}q_{fi} l_i$	Embank. $\sum_{i=1}^{N_2}q_{fi} l_i$	Geosyn. T_{rg}	Geosyn. T_{rp}	(Eq. 3)
D0	9.0	30.0	8.849	154.09	7.645	-	-	203.57	15.363	-	-	1.354
D1	8.5	28.5	7.558	150.30	6.362	5.119	62.413	202.28	14.327	50.0	433.39	1.507
D2	8.5	28.5	7.558	149.36	5.625	8.393	62.413	201.65	14.607	100.0	434.26	1.653
D3	9.0	29.0	10.123	212.53	3.791	9.772	66.726	312.60	14.573	150.0	500.03	1.755

R – radius; (X_0,Y_0) – coordinates of centre; $N=N_1+N_2$.

Table 7. Critical slip surfaces at the end of consolidation for cases D0-D3: overall safety factor (F) and sums of acting and resisting forces.

Case	X_0 (m)	Y_0 (m)	R (m)	Sum of acting forces (kN/m)			Geosyn. θ (°)	Sum of resisting forces (kN/m)				F
				Found. $\sum_{i=1}^{N_1}\tau_i l_i$	Embank. $\sum_{i=1}^{N_2}\tau_i l_i$	Geosyn. T_a		Found. $\sum_{i=1}^{N_1}q_{fi} l_i$	Embank. $\sum_{i=1}^{N_2}q_{fi} l_i$	Geosyn. T_{rg}	Geosyn. T_{rp}	(Eq. 3)
D0	9.5	28.0	6.536	124.45	2.680	-	-	181.68	15.506	-	-	1.551
D1	9.5	29.5	9.028	172.44	1.117	3.674	60.101	259.36	16.322	50.0	439.28	1.714
D2	8.5	28.5	7.558	149.70	3.096	8.714	62.413	233.92	15.216	100.0	433.92	1.884
D3	8.5	29.5	11.493	241.80	2.745	12.367	66.950	420.18	23.496	150.0	404.81	2.015

R – radius; (X_0,Y_0) – coordinates of centre; $N=N_1+N_2$.

factor. During the post-construction period, in response to consolidation, F increases in all cases, which is due to the increase of the soft soil strength as the excess pore pressure dissipates and effective mean stress increases.

Analysing the resisting forces of the geosynthetic at the cut point (Tables 6 and 7), one can conclude that T_{rg} is significantly smaller than T_{rp} in all cases. This means that the overall failure is determined by the geosynthetic strength and not by the pull-out strength of the soil-geosynthetic interfaces. Another conclusion is that the acting force of the geosynthetic at the cut point, T_a, is also significantly smaller than T_{rg} in all three cases (D1-D3). This reveals that the reserve of geosynthetic resistance remains high in all phases of the construction and post-construction periods, which justifies the larger values of the safety factor in cases D1-D3 than in case without geosynthetic (case D0).

Figure 16 shows the tensile force along the geosynthetic for cases D1-D3, at end of construction and end of consolidation. As expected, the higher the geosynthetic stiffness, the larger its tensile force (Borges, 1995; Borges & Cardoso, 2001). In all cases, due to the difference of deformability of soft soil and stone columns, tensile force is larger on the columns than on the nearby soft soil, both at the end of construction and end of consolidation. Another conclusion is that, after the end of construction, maximum values of tensile force do not significantly vary in response to consolidation; however, there is a decrease of tensile force in the spaces between columns, which is globally related with horizontal displacements of the geosynthetic during the post-construction period. In order to better understand such decrease, horizontal displacements at two points of the geosynthetic, corresponding to the extremities of the space between columns 2 and 3, for case D3, are indicated below: point A, with x-coordinate equal to 2.237 m; point B, with x-coordinate equal to 3.762 m. The following outward horizontal displacements were obtained at these two points: 1.43×10^{-2} m (end of construction) and

1.29×10^{-2} m (end of consolidation) for point A; 2.36×10^{-2} m (end of construction) and 2.15×10^{-2} m (end of consolidation) for point B. These results show that there is a shortening of the geosynthetic´s length between points A and B during the post-construction period; i.e., the average tensile strain of geosynthetic between such two points decreases after the end of construction and, therefore, so does the corresponding tensile force, as shown in Figure 16.

The following results are shown in Figures 17 and 18 for cases D0-D3: settlements on the embankment base (Figure 17); horizontal displacements under the embankment toe (Figure 18). These results reveal that the reinforcement with geosynthetic: (i) does not significantly influences the settlements on the embankment base, both at the end

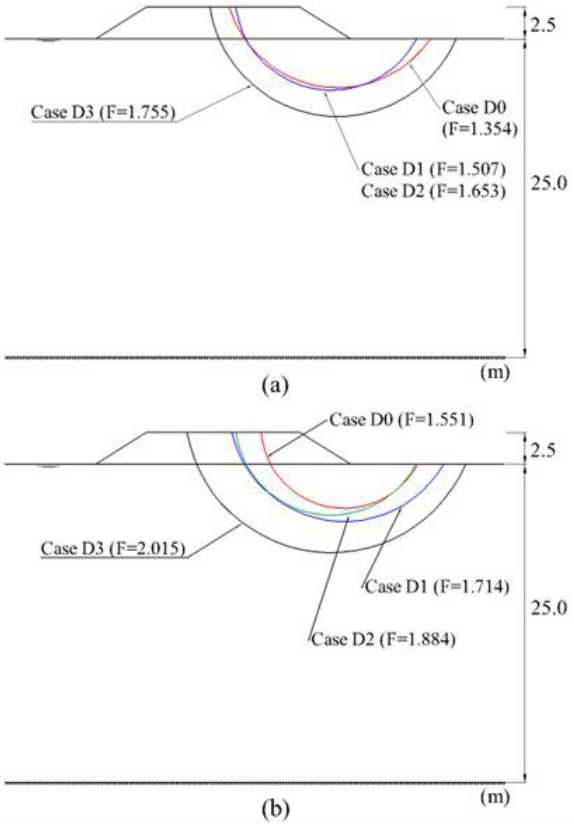

Figure 15. Critical slip surfaces for cases D0-D3: a) end of construction (7th day); b) end of consolidation.

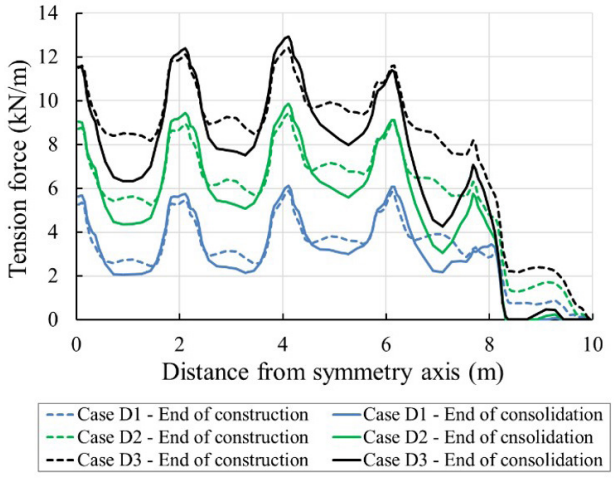

Figure 16. Geosynthetic tensile force for cases D1-D3, at end of construction and end of consolidation.

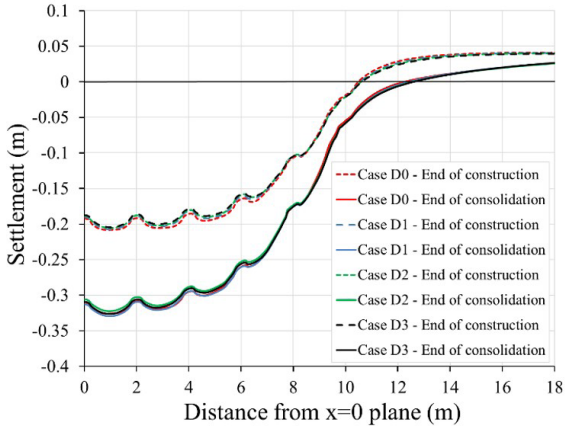

Figure 17. Vertical displacements on the ground surface (embankment base) for cases D0-D3, at the end of construction (7th day) and end of consolidation.

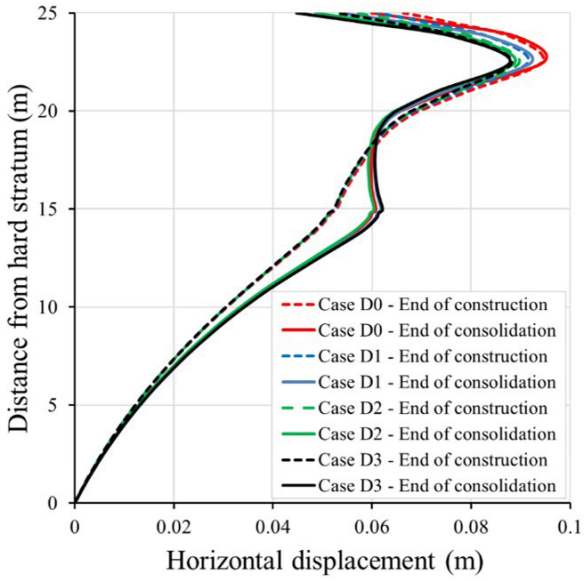

Figure 18. Horizontal displacements under the embankment toe (x =10 m) for cases D0-D3, at the end of construction (7th day) and end of consolidation.

of construction and end of consolidation; (ii) reduces a little the horizontal displacements under the embankment toe (on depths up to 3 m, approximately); the higher the geosynthetic stiffness, the larger this reduction, which is precisely explained by the increase of horizontal stiffness due to the inclusion of the geosynthetic. Another conclusion is that the horizontal displacements under the embankment toe do not significantly change after the end of construction in all cases, i.e. they are not significantly influenced by the consolidation process that takes place after the completion of the embankment. This globally explains that maximum values of tensile force in the geosynthetic also do not significantly change after the end of construction, as said above.

5. Conclusions

A parametric study was performed on the behaviour of a floating stone column-supported embankment on a thick soft soil deposit. Two parameters were studied: length of columns; basal reinforcement with geosynthetic (different constitutive curves for the geosynthetic were considered). The following overall conclusions are highlighted:

For values of *L/D* (ratio of the column length to the vertical thickness of soft soil) smaller than 0.6 approximately, the length of columns significantly influences the behaviour of problem, i.e. the longer the floating stone columns, the lower the settlements, the smaller the horizontal displacements, the higher the overall stability and the smaller the excess pore pressures at the end of construction, mainly below the end of columns. However, for values of *L/D* larger than 0.6, the study showed that increasing the length of columns does not significantly influence these parameters. This revealed that, also considering the cost, a length of columns between 10 m (*L/D*=0.4) and 15 m (*L/D*=0.6) would be adequate in practice for this problem. Another conclusion is that the length of columns does not significantly influence the load transfer to the top of columns during construction.

Regarding the influence of reinforcement with geosynthetic, the study showed that: (i) the safety factor (*F*) at the end of construction significantly increases when a geosynthetic is included on the embankment base; (ii) as expected, the higher the geosynthetic strength, the higher the safety factor. On the other hand, settlements on the embankment base are not significantly influenced by the geosynthetic inclusion, both at the end of construction and at the end of consolidation. Another conclusion is that the horizontal displacements under the embankment toe reduce a little with the geosynthetic reinforcement; the higher the geosynthetic stiffness, the larger this reduction. Due to the difference of deformability of soft soil and stone columns, the geosynthetic tensile force is larger on the stone columns than on the nearby soft soil. The higher the geosynthetic stiffness, the larger its tensile force, as expected.

Acknowledgements

This work was financially supported by: Base Funding - UIDB/04708/2020 of the CONSTRUCT - Instituto de I&D em Estruturas e Construções - funded by national funds through the FCT/MCTES (PIDDAC).

Declaration of interest

The author has no conflicts of interest to declare.

Data availability

All data of the current study are included in this article.

List of symbols

a_s	area replacement factor
c_r	reduction coefficient
f	yielding function
h	hardening parameter
k	slope of swelling and recompression line
k_h	coefficient of permeability in horizontal direction
k_v	coefficient of permeability in vertical direction
l_i	*i*-segment length
p	effective mean stress
q	deviatoric stress
q_{fi}	average value of soil shear strength at *i*-segment
s	axis-to-axis spacing between columns
s_p	plastic tangential relative displacement
u	excess pore pressure
v_i	soil specific volume at *i*-segment
A_c	column area
A_t	tributary area of natural soil for each column
D	vertical thickness of soft soil
F	overall safety factor
L	length of columns
M	slope of the critical state line
N	specific volume of normally consolidated soil at mean normal stress equal to 1 kPa
N	number of 2D elements of the mesh intersected by the slip circle
N_g	number of geosynthetic layers
T_{aj}	acting tensile force of *j*-geosynthetic at the cut point
T_{rg}	geosynthetic strength
T_{rp}	pull-out strength of the soil-geosynthetic interface
T_{rj}	resisting tensile force of *j*-geosynthetic at cut point
Y	hardening law
α_p	*p*-value of yield surface centre in *p-q* plane
γ	unit weight
δ	interface friction angle
ε_p	plastic tensile strain
θ	angular stress invariant

θ_j angle between the *j*-geosynthetic and the tangent to the slip circle at the cut point
λ slope of normal consolidation line and critical state line
ν' Poisson's ratio for drained loading
σ tensile stress
σ_n normal stress
σ'_x effective normal stress in *x*-direction
σ'_y effective normal stress in *y*-direction
σ_Y yielding stress
σ'_z effective normal stress in *z*-direction
τ tangential stress
τ_i average value of acting shear stress at *i*-segment
τ_{xy} shear stresses in *xy*-plane
ϕ' angle of friction defined in effective terms
Γ specific volume of soil on the critical state line at mean normal stress equal to 1 kPa

References

Abusharar, S.W., & Han, J. (2011). Two-dimensional deep-seated slope stability analysis of embankments over stone column-improved soft clay. *Engineering Geology*, 120(1-4), 103-110. http://dx.doi.org/10.1016/j.enggeo.2011.04.002.

Almeida, M.S.S., Hosseinpour, I., Riccio, M., & Alexiew, D. (2015). Behavior of geotextile encased granular columns supporting test embankment on soft deposit. *Journal of Geotechnical and Geoenvironmental Engineering*, 141(3), 129-139. http://dx.doi.org/10.1061/(ASCE)GT.1943-5606.0001256.

Basack, S., Indraratna, B., Rujikiatkamjorn, C., & Siahaan, F. (2017). Modeling the stone column behavior in soft ground with special emphasis on lateral deformation. *Journal of Geotechnical and Geoenvironmental Engineering*, 143, 04017016. http://dx.doi.org/10.1061/(ASCE)GT.1943-5606.0001652.

Borges, J.L. (1995). *Geosynthetic-reinforced embankments on soft soils - Analysis and design* [Doctoral thesis, University of Porto]. University of Porto's repository (in Portuguese). Retrieved in May 16, 2023, from http://hdl.handle.net/10216/11931

Borges, J.L. (2004). Three-dimensional analysis of embankments on soft soils incorporating vertical drains by finite element method. *Computers and Geotechnics*, 31(8), 665-676. http://dx.doi.org/10.1016/j.compgeo.2004.11.001.

Borges, J.L. (2022). Vacuum preloading and PVDs in soft soils beneath embankments: 3D coupled analysis incorporating overall stability study. *Soils and Rocks*, 45(3), e2022072821. http://dx.doi.org/10.28927/SR.2022.072821.

Borges, J.L., & Almeida, F. (2018). Sidewalls and PVDs below embankments on soft soils – three-dimensional analysis by FEM. *Geosynthetics International*, 25(6), 630-643. http://dx.doi.org/10.1680/jgein.18.00030.

Borges, J.L., & Cardoso, A.S. (2001). Structural behaviour and parametric study of reinforced embankments on soft clays. *Computers and Geotechnics*, 28(3), 209-233. http://dx.doi.org/10.1016/S0266-352X(00)00021-5.

Borges, J.L., & Cardoso, A.S. (2002). Overall stability of geosynthetic-reinforced embankments on soft soils. *Geotextiles and Geomembranes*, 20(6), 395-421. http://dx.doi.org/10.1016/S0266-1144(02)00014-6.

Borges, J.L., & Gonçalves, M.S. (2016). Jet-grout column-reinforced soft soils incorporating multilayer geosynthetic-reinforced platforms. *Soil and Foundation*, 56(1), 57-72. http://dx.doi.org/10.1016/j.sandf.2016.01.005.

Borges, J.L., & Guerra, G.T. (2014). Cylindrical excavations in clayey soils retained by jet grout walls: numerical analysis and parametric study considering the influence of consolidation. *Computers and Geotechnics*, 55, 42-56. http://dx.doi.org/10.1016/j.compgeo.2013.07.008.

Borges, J.L., & Marques, D.O. (2011). Geosynthetic-reinforced and jet grout column-supported embankments on soft soils: numerical analysis and parametric study. *Computers and Geotechnics*, 38(7), 883-896. http://dx.doi.org/10.1016/j.compgeo.2011.06.003.

Borges, J.L., & Santos, R.M. (2020). Bottom reinforcement in braced excavations: coupled analysis and new method for basal-heave stability study. *Soils and Rocks*, 43(2), 199-217. http://dx.doi.org/10.28927/SR.432199.

Borges, J.L., Domingues, T.S., & Cardoso, A.S. (2009). Embankments on soft soil reinforced with stone columns: numerical analysis and proposal of a new design method. *Geotechnical and Geological Engineering*, 27(6), 667-679. http://dx.doi.org/10.1007/s10706-009-9266-z.

Britto, A.M., & Gunn, M.J. (1987). *Critical soil mechanics via finite elements*. Ellis Horwood Limited.

Castro, J. (2017). Groups of encased stone columns: influence of column length and arrangement. *Geotextiles and Geomembranes*, 45(2), 68-80. http://dx.doi.org/10.1016/j.geotexmem.2016.12.001.

Castro, J., & Sagaseta, C. (2011). Deformation and consolidation around encased stone columns. *Geotextiles and Geomembranes*, 29(3), 268-276. http://dx.doi.org/10.1016/j.geotexmem.2010.12.001.

Castro, J., Cimentada, A., da Costa, A., Cañizal, J., & Sagaseta, C. (2013). Consolidation and deformation around stone columns: comparison of theoretical and laboratory results. *Computers and Geotechnics*, 49, 326-337. http://dx.doi.org/10.1016/j.compgeo.2012.09.004.

Chen, J., Zhang, X., Yoo, C., & Gu, Z. (2022). Effect of basal reinforcement on performance of floating geosynthetic encased stone column-supported embankment. *Geotextiles and Geomembranes*, 50(4), 566-580. http://dx.doi.org/10.1016/j.geotexmem.2022.01.006.

Chen, R.P., Chen, Y.M., Han, J., & Xu, Z.Z. (2009). A theoretical solution for pile supported embankments on soft soils under one-dimensional compression. *Canadian*

Geotechnical Journal, 45(5), 611-623. http://dx.doi.org/10.1139/T08-003.

Christoulas, S., Giannaros, C., & Tsiambaos, G. (1997). Stabilization of embankment foundations by using stone columns. *Geotechnical and Geological Engineering*, 15(3), 247-258. http://dx.doi.org/10.1007/BF00880828.

Cooper, M.R., & Rose, A.N. (1999). Stone column support for an embankment on deep alluvial soils. *Proceedings of the Institution of Civil Engineers: Geotechnical Engineering*, 37(1), 15-25. http://dx.doi.org/10.1680/gt.1999.370103.

Costa, P.A. (2005). *Braced excavations in soft clayey soils: Behavior analysis including the consolidation effects* [MSc thesis, University of Porto]. University of Porto's repository (in Portuguese). Retrieved in May 16, 2023, from http://hdl.handle.net/10216/12092

Costa, P.A., Borges, J.L., & Fernandes, M.M. (2007). Analysis of a braced excavation in soft soils considering the consolidation effect. *Geotechnical and Geological Engineering*, 25(6), 617-629. http://dx.doi.org/10.1007/s10706-007-9134-7.

Deb, K., Samadhiya, N.K., & Namdeo, J.B. (2011). Laboratory model studies on unreinforced and geogrid-reinforced sand bed over stone column-improved soft clay. *Geotextiles and Geomembranes*, 29(2), 190-196. http://dx.doi.org/10.1016/j.geotexmem.2010.06.004.

Domingues, T.S. (2006). *Foundation reinforcement with stone columns in embankments on soft soils: analysis and design*. [MSc thesis, University of Porto]. University of Porto's repository (in Portuguese). Retrieved in May 16, 2023, from http://hdl.handle.net/10216/11226

Elsawy, M.B.D. (2013). Behaviour of soft ground improved by conventional and geogrid-encased stone columns, based on FEM study. *Geosynthetics International*, 20(4), 276-285. http://dx.doi.org/10.1680/gein.13.00017.

Finno, R.J., Harahap, I.S., & Sabatini, P.J. (1991). Analysis of braced excavations with coupled finite element formulations. *Computers and Geotechnics*, 12(2), 91-114. http://dx.doi.org/10.1016/0266-352X(91)90001-V.

Lewis, R.W., & Schrefler, B.A. (1987). *The finite element method in the deformation and consolidation of porous media*. John Wiley and Sons, Inc..

Marandi, S.M., Anvar, M., & Bahrami, M. (2016). Uncertainty analysis of safety factor of embankment built on stone column improved soft soil using fuzzy logic α-cut technique. *Computers and Geotechnics*, 75, 135-144. http://dx.doi.org/10.1016/j.compgeo.2016.01.014.

Marques, D.O. (2008). *Reinforcement of foundation soils with jet-grout columns and geosynthetics* [MSc thesis, University of Porto]. University of Porto's repository (in Portuguese). Retrieved in May 16, 2023, from http://hdl.handle.net/10216/58775

Marques, D.O. (2021). *Embankments on soft soils reinforced with stone columns: numerical and experimental analysis* [Doctoral thesis, University of Porto]. University of Porto's repository (in Portuguese). Retrieved in May 16, 2023, from https://hdl.handle.net/10216/134157

Marques, D.O., & Borges, J.L. (2018a). Stone column-supported embankments on soft soils: Three-dimensional analysis through the finite element method. In *NUMGE 2018 - 9th European Conference on Numerical Methods in Geotechnical Engineering* (pp. 1407-1414), Porto, Portugal. Porto: FEUP Publisher. https://doi.org/10.1201/9781351003629.

Marques, D.O., & Borges, J.L. (2018b). Three-dimensional parametric study of stone column-supported embankments on soft soils. In *NUMGE 2018 - 9th European Conference on Numerical Methods in Geotechnical Engineering* (pp. 1415-1422). Porto, Portugal. Porto: FEUP Publisher. https://doi.org/10.1201/9781351003629.

Miranda, M., Fernández-Ruiz, J., & Castro, J. (2021). Critical length of encased stone columns. *Geotextiles and Geomembranes*, 49(5), 1312-1323. http://dx.doi.org/10.1016/j.geotexmem.2021.05.003.

Owen, D.R.J., & Hinton, E. (1980). *Finite elements in plasticity: theory and practice.* Pineridge Press Limited.

Prevost, J.H., & Hoeg, K. (1975). Effective stress-strain-strength model for soils. *Journal of the Geotechnical Engineering Division*, 101(GT3), 259-278.

Rowe, R.K., & Li, A.L. (2005). Geosynthetic-reinforced embankments over soft foundations. *Geosynthetics International*, 12(1), 50-85. http://dx.doi.org/10.1680/gein.2005.12.1.50.

Rowe, R.K., & Soderman, K.L. (1985). An approximate method for estimating the stability of geotextile-reinforced embankments. *Canadian Geotechnical Journal*, 22(3), 392-398. http://dx.doi.org/10.1139/t85-050.

Rowe, R.K., & Soderman, K.L. (1987). Stabilization of very soft soils using high strength geosynthetics: the role of finite element analyses. *Geotextiles and Geomembranes*, 6, 53-80. http://dx.doi.org/10.1016/0266-1144(87)90057-4.

Tan, S., Tjahyono, S., & Oo, K. (2008). Simplified plane-strain modeling of stone-column reinforced ground. *Journal of Geotechnical and Geoenvironmental Engineering*, 134, 185-194. http://dx.doi.org/10.1061/(ASCE)1090-0241(2008)134:2(185).

Thomas, J.N. (1984). An improved accelerated initial stress procedure for elasto-plastic finite element analysis. *International Journal for Numerical and Analytical Methods in Geomechanics*, 8, 359-379. http://dx.doi.org/10.1002/nag.1610080405.

Zhang, X., Yoo, C., Chen, J., & Gu, Z. (2022). Numerical modeling of floating geosynthetic-encased stone column–supported embankments with basal reinforcement. *Geotextiles and Geomembranes*, 50(4), 720-736. http://dx.doi.org/10.1016/j.geotexmem.2022.03.012.

Zhang, Z., Han, J., & Ye, G. (2014). Numerical investigation on factors for deep-seated slope stability of stone column-supported embankments over soft clay. *Engineering Geology*, 168, 104-113. http://dx.doi.org/10.1016/j.enggeo.2013.11.004.

Zhao, L., Zhou, W., Geng, X., Yuen, K., & Fatahi, B. (2019). A closed-form solution for column-supported embankments with geosynthetic reinforcement. *Geotextiles and Geomembranes*, 47(3), 389-401. http://dx.doi.org/10.1016/j.geotexmem.2019.01.006.

Zhou, Y., Kong, G., Zheng, J., Wen, L., & Yang, Q. (2021). Analytical solutions for geosynthetic-encased stone column-supported embankments with emphasis on nonlinear behaviours of columns. *Geotextiles and Geomembranes*, 49(5), 1107-1116. http://dx.doi.org/10.1016/j.geotexmem.2021.03.005.